Numerical investigation on the Thermal-hydraulic performance of the modified channel supercritical CO_2 printed circuit heat exchanger

Wang, Jian; Yan, Xin ping; Boersma, Bendiks J.; Lu, Ming jian; Liu, Xiaohua

DOI
10.1016/j.applthermaleng.2022.119678

Publication date
2023

Document Version
Final published version

Published in
Applied Thermal Engineering

Applied Thermal Engineering 221 (2023) 119678

Contents lists available at ScienceDirect

Applied Thermal Engineering

journal homepage: www.elsevier.com/locate/apthermeng

Numerical investigation on the Thermal-hydraulic performance of the modified channel supercritical CO_2 printed circuit heat exchanger

Jian Wang [a,b,c], Xin-ping Yan [a,b], Bendiks J. Boersma [c], Ming-jian Lu [a,b,*], Xiaohua Liu [a,b]

[a] School of Transportation and Logistics Engineering, Wuhan University of Technology, Hubei, Wuhan, 430063, China
[b] Reliability Engineering Institute, National Engineering Research Center for Water Transport Safety, MoST, Hubei, Wuhan, 430063, China
[c] Process & Energy Department, Faculty of Mechanical, Maritime and Materials Engineering, Delft University of Technology, the Netherlands

ARTICLE INFO

Keywords:
Printed circuit heat exchanger
Heat transfer
Supercritical carbon dioxide
CFD
Modified channel

ABSTRACT

Printed circuit heat exchangers (PCHE) are designed to improve heat recovery and energy saving in supercritical CO_2 (S-CO_2) power cycles. In the current study, a modified channel PCHE is proposed based on the regular straight channel and a zigzag channel. The thermal–hydraulic performance of four different types of PCHE is numerically investigated and the methods are verified by both experimental and numerical results. The numerical results are presented for a Reynolds number based on the inlet conditions between 5 000 and 25 000. From the numerical results, the local pressure loss and local heat transfer coefficients are analyzed and discussed. Subsequently, the global Nusselt number and Fanning friction coefficients are discussed. It is found that the inserted straight section contributes to uniform flow, resulted in significant pressure loss reduction with a slight decrease in heat transfer. The modified channel can reduce the Fanning friction coefficient by 33.1%-84.7% while the global Nusselt number reduction is about 3.6%-30.3%. This leads to a maximum performance evaluation criterion (PEC) enhancement of 45.9%.

1. Introduction

With the intensification of the worldwide environmental crisis and energy shortage, demands for more efficient and sustainable energy solutions and power generation technologies are an urgent problem. Interest in alternative power conversion systems is increasing to successfully utilize new energy sources or to improve the efficiency of traditional systems. In recent years, supercritical CO_2 (S-CO_2) Brayton cycles have gained attention due to its small footprint and high thermodynamic compared to other power systems. Several investigations have been carried out to study the possibility of the S-CO_2 power systems, such as the "Generation IV" nuclear reactor [1], coal-fired power plants [2,3], concentrated solar power plant technology [4,5], and industrial waste heat recovery systems [6,7]. One of the most critical components in the S-CO_2 power cycles is the compact heat exchanger [8].

A printed circuit heat exchanger (PCHE), which was initially commercialized by the Heatric Company [9], is a promising alternative for the heat exchanger in S-CO_2 cycles because of its high heat transfer efficiency and structural rigidity. Generally, PCHE consists of a heat exchanger core and headers. The core is fabricated from a stack of mm-thickness plates with regular chemically-etched micro semi-circular channels, as shown in Fig. 1(a). The plates are joined together by a diffusion bonding technique with a prescribed configuration to separate hot and cold fluids. Then the flow distribution headers as inlets and outlets are welded to the core. Recently, PCHE has attracted considerable attention in some potential applications fields due to its excellent performance [8,10].

Numerous experimental investigations have been conducted to clarify the thermal–hydraulic characteristics of PCHEs. Chu et al. [11,12] tested the independent manufactured straight channel and zigzag channel PCHEs using S-CO_2 and water as working fluids. The results showed that the thermal–hydraulic performance was related to working fluids, operating conditions, and pitch angles marked as θ in Fig. 1(c). Seo et al. [13] experimentally investigated the heat transfer and pressure drop characteristics of straight channel PCHE in the laminar flow regime and proposed relevant correlations. Pra et al. [14] found that the zigzag channel PCHE had no heat transfer enhancement at a low Reynolds number regime compared with the straight channels based on the experimental data. Ngo et al. [15] investigated the heat transfer and pressure drop characteristics of the zigzag channel and S-shaped fins PCHEs in an experimental S-CO_2 loop. The results indicated that the Nusselt number of the zigzag channels was 24–34 % higher than

* Corresponding author at: Reliability Engineering Institute, School of Energy and Power Engineering, Wuhan University of Technology, Hubei, China.
E-mail address: mingjian_lu@whut.edu.cn (M.-j. Lu).

https://doi.org/10.1016/j.applthermaleng.2022.119678
Received 14 September 2020; Received in revised form 11 April 2022; Accepted 14 November 2022
Available online 26 November 2022

Nomenclature

A_c	area of cross-section (mm^2)
C_p	specific heat (kJ/kg/K)
D_h	hydraulic diameter(mm)
d	channel diameter (mm)
f	Fanning friction factor
h	convection heat transfer coefficient
k	turbulent kinetic energy (m^2/s^2)
L	Length of the centerline (mm)
m	mass flow rate (kg/s)
Nu	Nusselt number
max	maximum value
min	minimum value
Δp	local pressure loss (Pa)
P	pressure (bar)
PCHE	printed circuit heat exchanger
PEC	performance evaluation criteria
q	heat flux (W/m^2)
Re	Reynolds number
T	temperature (K)
W	wetted perimeter (mm)

Greek letters

δ	ratio of inserted straight section
θ	zigzag pitch angle (°)
ρ	density (kg/m^3)
λ	thermal conductivity (W/m/K)
μ	dynamic viscosity (Pa·s)
χ	relative position in the sixth pitch

Subscripts

b	bulk
c	cold side
h	hot side
in	inlet
o	overall
M	modified channel
out	outlet
S	sinusoidal channel
Str	straight channel
w	wall
Z	zigzag channel

that of S-shaped fins, but the pressure loss was 4–5 times larger. Chen and Sun et al. [16–18] investigated the thermal–hydraulic performance of a zigzag channel PCHE with a pitch angle of 15° on the high-temperature helium facility at The Ohio State University. The results indicated that although the zigzag channels had better overall heat transfer performance, the Fanning friction factors of the zigzag channel were 2–3 times those in the straight circular pipes in the laminar flow regime. Zhao et al. [19] conducted experimental research on the thermal–hydraulic performance of supercritical nitrogen PCHE with airfoil fins channel. New correlations of the Fanning friction factor and Nusselt number were developed for the airfoil PCHE with supercritical nitrogen as the working fluid. Zhou and Cheng et al. [20,21] tested two 100 kW class PCHE prototypes for the S-CO_2 Brayton cycle, as recuperator and precooler respectively. It was found that heat transfer effectiveness σ was in the range 95 %-98.4 % and the pressure drop ΔP was less than 48 kPa on both sides, which could meet the design requirements(σ ≥ 92%, $\Delta P \leq 250$ kPa). Park at al. [22] conducted experimental examination of the thermal–hydraulic performance of a 3 kW PCHE as a precooler. It was found that the thermo-physical properties significantly affected the change in Nusselt number based on flow direction when S-CO_2 was operated under near-critical and *trans*-critical conditions, which should be considered in the design of PCHE for the precooler.

Various numerical simulations were widely promoted to seek better thermal–hydraulic performance of PCHE with continuous channels [23–25] for instance straight channel, zigzag channel, and sinusoidal channel. Lee and Kim et al. [26–28] studied the effects of the geometry parameters on the thermal–hydraulic characteristics of zigzag channel PCHE. The zigzag channel showed the best flow characteristics when the pitch angle was 0° and the best thermal performance when the pitch angle was 35°. Wen et al. [29] investigated the effects of geometric parameters on the thermal–hydraulic performance of sinusoidal channel PCHE and found that the amplitude and wavy-length changes led to the

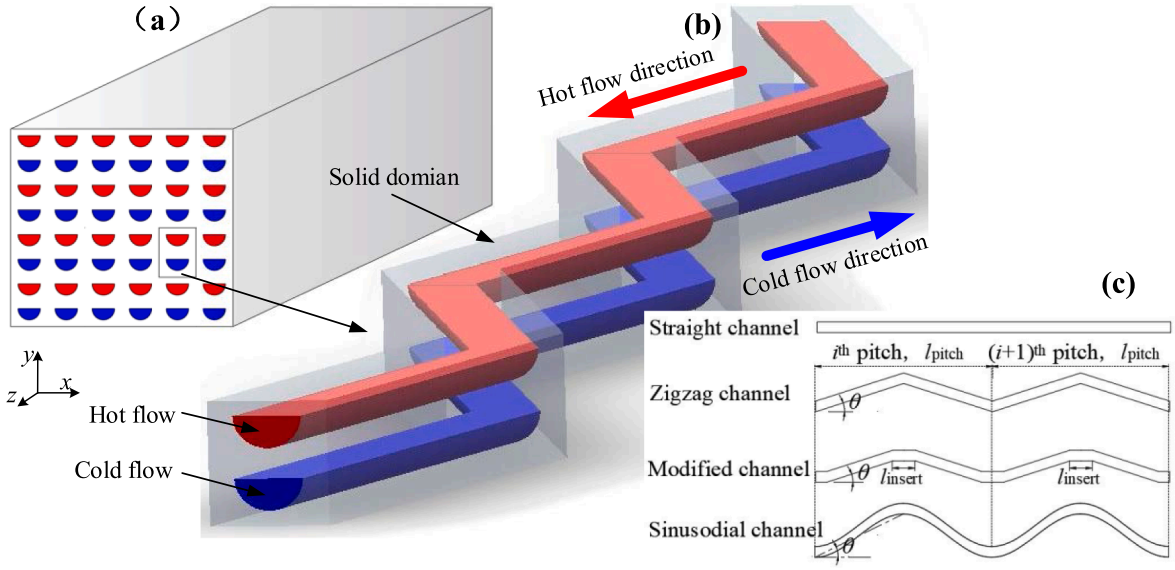

Fig. 1. Physical model of PCHE.

change of centrifugal forces and heat flux distributions which would further affect the overall performance. A comparison investigation between the sinusoidal channel and the zigzag channel was conducted by Aneesh et al. [30] and the computational results showed that the sinusoidal channel had better comprehensive performance than the zigzag one. As a kind of the discontinuous fins PCHEs, the S-shaped fins PCHE was originally introduced by Tsuzuki et al. [31]. Their numerical results showed that the S-shaped fins could decrease the pressure drop by 20 % that of the zigzag channel while giving identical heat transfer performance. The airfoil fins PCHE was also widely investigated. Zhao et al. [32] studied the effect of multiple parameters including the horizontal spacing, vertical spacing, staggered spacing, and airfoil fins arrangements on the flow and heat transfer performance of PCHE. Their analysis showed that a sparser staggered arrangement was suggested to enhance the comprehensive performance of PCHE, which was also recommended by Kim et al. [33] coincidentally. Chu et al. [34] studied the geometrical parameters of airfoil fins and concluded that fins with the large windward area and short length could lead to a better comprehensive performance PCHE. Cui et al. [35] proposed two novel fins based on the regular airfoil NACA 0020 fin. The results indicated that one of the novel fins had better heat transfer and flow performance than the regular one.

Despite a number of studies on various channels PCHE, the zigzag channel is still the most frequently used type due to the mature manufacturing process and large heat transfer capability [8]. Baik et al. [36] replaced the sharp corner of the zigzag channel with a rounded corner and found that a 40 %-65 % reduction of pressure drop. To improve the performance of the zigzag channel PCHE, Lee et al. [37] suggested a new type of PCHE with inserted straight channels at the bending points to reduce the huge pressure drop. Numerical results showed that the inserted straight section could reduce the Fanning friction coefficient by 60 % among all conditions. Meanwhile, it could keep a similar thermal performance with the zigzag channel. Resulting in a volume-goodness factor promotion of 26 %-28 % over the zigzag channel. Aneesh et al. [30] numerically investigated the thermal–hydraulic characteristics of three wavy channels, at the laminar flow region. The trapezoidal channel, the sinusoidal channel, and the triangular channel showed a heat transfer enhancement ratio of 41 %, 33 %, and 28 % compared with the straight channel, respectively. The trapezoidal channel could offer the best heat transfer performance with the largest pressure loss penalty. The channels mentioned by Lee [37] and Aneesh [30] can be collectively referred to as the modified channel based on the zigzag channel. It can be concluded that the modified channel remains competitive in all wavy channels. However, the thermal–hydraulic performance of the modified channel PCHE with S-CO_2 flow is not involved in the previous research. And there is no study which focused on the effect of geometrical parameters on the thermal–hydraulic performance of the modified channel PCHE at the transition or turbulence flow region.

Therefore, further work should be done to investigate the thermal–hydraulic performance of the modified channel PCHE with S-CO_2 in the transition or turbulent regime (Re = 5 000–25 000). A total of sixteen channel configurations are involved in the current study, including one straight channel, three zigzag channels, three sinsodial channels and nine modified channels. The numerical model is firstly verified by both experimental and simulation results. Then the local flow and heat transfer characteristics of the modified channel in a pitch along the flow direction of channels are analyzed. Next, the global Nusselt number and Fanning friction coefficient of all cases are discussed and compared. At last, the comprehensive performance of all channels is evaluated under different operating conditions and the optimum geometry configuration is suggested.

2. Numerical simulations

2.1. Physical model

PCHE consists of several heat transfer plates which are stacked together with alternating hot and cold aisle arrangement configuration, as shown in Fig. 1(a). Therefore, a simplified periodic unit showing as Fig. 1(b) with hot fluid-cold fluid counter-flow arrangement can be used in PCHEs' numerical investigation. In Fig. 1(c) the four different geometrical configurations employed in this study, straight channel, zigzag channel, the combination of them, modified channel and sinsodial channel are presented.

For the modified channel it is convenient to introduce a new parameter of the inserted-straight section ratio. The ratio is defined as follows:

$$\delta = \frac{2l_{insert}}{l_{pitch}} \tag{1}$$

Where, l_{pitch} is the pitch length; l_{insert} is the insert straight section length at each bend and 2 l_{insert} represents the total length of the insert straight section in one pitch. In particular, when δ is equal to 0 and 1, it represents the zigzag channel and straight channel respectively. Detailed geometrical characteristics for all cases of channel configurations used for simulation in the present work are shown in Table 1. For a straight channel, we define the bend angle as 0. For the zigzag channels and modified channels, the bend angle is in the range of 15° to 45°. Each model consists of 12 pitches and each pitch's projection length is 24.6 mm which is recommended by Heatric and others [38,39]. In Fig. 2, the cross-section of the simplified model is shown. It has a semicircle channel diameter d = 2 mm, an adjacent pitch *width* = 3 mm, and a thickness of plate *height/2* = 2 mm. The total projection length of all cases is 295.2 mm, while the total centerline length of different channels varies from 295.2 mm to 417.5 mm.

2.2. Governing equations

In this study, the 3D steady-state and incompressible fluid flow is assumed. The continuity, momentum, and energy equation governing the 3D steady flow are as follows [40]:

Continuity:

$$\frac{\partial}{\partial x_i}(\rho u_i) = 0 \tag{2}$$

Momentum:

$$\frac{\partial}{\partial x_i}\left(\rho u_i u_j\right) = \frac{\partial}{\partial x_i}\left[(\mu + \mu_t)\left(\frac{\partial u_i}{\partial x_j} + \frac{\partial u_j}{\partial x_i}\right) - \frac{2}{3}(\mu + \mu_t)\frac{\partial u_k}{\partial x_k}\right] - \frac{\partial p_i}{\partial x_i} \tag{3}$$

Table 1
Geometrical characteristics of different cases of PCHE.

Case	θ(°)	δ	Type	Group
Str	0	1	Straight channel	
S15	/	/	Sinusodial channel	1
Z15	15	0	Zigzag channel	
M15-0.2	15	0.2	Modified channel	
M15-0.4	15	0.4	Modified channel	
M15-0.6	15	0.6	Modified channel	
S30	/	/	Sinusodial channel	2
Z30	30	0	Zigzag channel	
M30-0.2	30	0.2	Modified channel	
M30-0.4	30	0.4	Modified channel	
M30-0.6	30	0.6	Modified channel	
S45	/	/	Sinusodial channel	3
Z45	45	0	Zigzag channel	
M45-0.2	45	0.2	Modified channel	
M45-0.4	45	0.4	Modified channel	
M45-0.6	45	0.6	Modified channel	

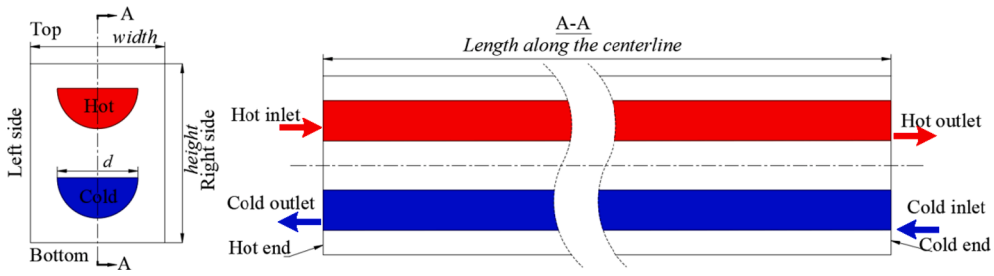

Fig. 2. Double bank channel unit for simulation.

Energy:

$$\frac{\partial}{\partial x_i}(\rho u_i C_p T) = \frac{\partial}{\partial x_i}\left(\lambda \frac{\partial T}{\partial x_j}\right) + \Phi \tag{4}$$

where ρ, u, μ, μ_t, C_p, λ, and T are the Favre averaged density, velocity, dynamic viscosity, turbulent viscosity, specific heat, thermal conductivity, and temperature of the fluid, respectively. Φ is the energy dissipation due to the viscosity of working fluids. The Shear Stress Transport (SST) k–ω model is employed to solve the turbulent flow and conjugate heat transfer in counter-flow microchannel PCHE. Because SST k–ω model combines the robustness of k-ω in the near-wall region and the accuracy of k-ε far from the wall, therefore gives more accurate predictions about the thermal dynamic performance of supercritical fluids with variable properties than the standard k-ε model. The turbulence kinetic energy k and the specific dissipation rate ω are obtained from the following transport equations:

$$\frac{\partial}{\partial t}(\rho k) + \frac{\partial}{\partial x_i}(\rho k u_i) = \frac{\partial}{\partial x_j}\left(\Gamma_k \frac{\partial k}{\partial x_j}\right) + G_k - Y_k \tag{5}$$

$$\frac{\partial}{\partial t}(\rho \omega) + \frac{\partial}{\partial x_i}(\rho \omega u_i) = \frac{\partial}{\partial x_j}\left(\Gamma_\omega \frac{\partial k}{\partial x_j}\right) + G_\omega - Y_\omega \tag{6}$$

In the equations, G_k represents the generation of turbulence kinetic energy due to mean velocity gradients. G_ω represents the generation of ω. Γ_k and Γ_ω represent the effective diffusivity of k and ω, respectively. Y_k and Y_ω represent the dissipation of k and ω due to turbulence. All the governing equations are solved using the second-order upwind scheme. The semi-implicit method pressure linked equation (SIMPLE) was used for coupling velocity to pressure. The computational domain contains five boundary conditions as presented in Table 2. Both inlets are set as a fixed mass flow rate and the outlets are set as constant pressure boundary conditions. PCHE contains several periodic heat transfer channels, so periodic boundary conditions are applied to the top and bottom walls in the simulation model, as well as to the left and right sides. The fluid domain and solid domain are connected by an interface. Moreover, the remainder outside walls of the solid domain are treated as adiabatic to avoid extra heat loss. All the operating conditions for this study are shown in Table 3. The Reynolds number at both inlets varies from 5000 to 25,000 with a step of 5000, which is expressed as

$$Re = \frac{\rho u D_h}{\mu} = \frac{m D_h}{A_c \mu} \tag{7}$$

Where ρ, u, andμ are the density, velocity, dynamic viscosity of S-CO_2 at the inlets, respectively. A_c is the cross-sectional area and m is the mass flow rate. D_h is the hydraulic diameter of the channel which is obtained by

$$D_h = \frac{4A_c}{W} \tag{8}$$

where W is the wetted perimeter cross-sectional.

Type 316 L Stainless Steel is utilized as the construction material for the heat exchanger core due to its corrosion resistance. The density, specific heat, and thermal conductivity are 8238 kg/m^3, 0.468 kJ/kg·K, and 16.2 W/m·K, respectively. The thermodynamic and transport properties of the working fluid, S-CO_2, are calculated using the NIST Standard Reference Database [41].

Table 2
Boundary conditions.

Domain	Name	Boundary condition
Fluid (S-CO_2)	Inlet	Mass flow rate
	Outlet	Pressure outlet
Solid (316 L)	Top wall & Bottom wall	Periodic($q_{top} = -q_{bottom}$)
	Left side & Right side	Periodic($q_{left} = -q_{right}$)
	End walls	Adiabatic($q_{end} = 0$)

Table 3
Operating conditions employed in the present study.

	Inlet temperature (K)	Operating pressure (bar)	Mass flow rate range (kg/s)	Re
Hot flow	651	90.6	1.97×10^{-4}-9.83×10^{-4}	5 000–25 000
Cold flow	385	148.5	1.69×10^{-4}-8.5 $\times 10^{-4}$	5 000–25 000

2.3. Grid generation and independence test

To determine the optimum number of meshes, the case θ45δ0 with the sharpest bends and the length along the centerline of 417.5 mm is chosen as a representative model. Because sharper bends along the flow direction can lead to a decrease in the convergence of the solution or even to its loss. A high-quality block-structural mesh is generated by ANSYS ICEM CFD to ensure simulation accuracy. An O-type grid is created separately for the fluids and solid domains to improve the quality of the mesh. The grid independence test is carried out for the simplified PCHE model by constantly adjusting the number of elements of cross-section and flow direction. The results are shown in Fig. 3; calculated for $Re_{c,in} = Re_{h,in} = 5 \times 10^3$, accordingly, $m_{c,in} = 1.69 \times 10^{-4}$ kg/s, $m_{h,out} = 1.97 \times 10^{-4}$ kg/s. As the number of elements reaches to 3 217 484, outlet temperature and pressure drop at both sides converge faultlessly. The structured grid system used in the present study is shown in Fig. 4. 15 sheets of boundary grids with a growth rate of 1.2 are produced near the fluid wall connected with the solid domain, and the first node adjacent to the wall is 0.01 mm. The distributions of grid nodes on the cross-section are exactly the same in all models. The grid size is defined as 5×10^{-3} mm along the flow direction. Hence, the number of elements varies from 2.26 million to 3.22 million due to the different travel lengths among all the cases.

2.4. Code verification

The numerical model is validated using the zigzag channel PCHE experiment in the KAIST helium test loop reported as by Kim et al.[42]. Details about the experiment and operating conditions can be found in [43]. The geometry model is in line with including the bend angle of 15°,

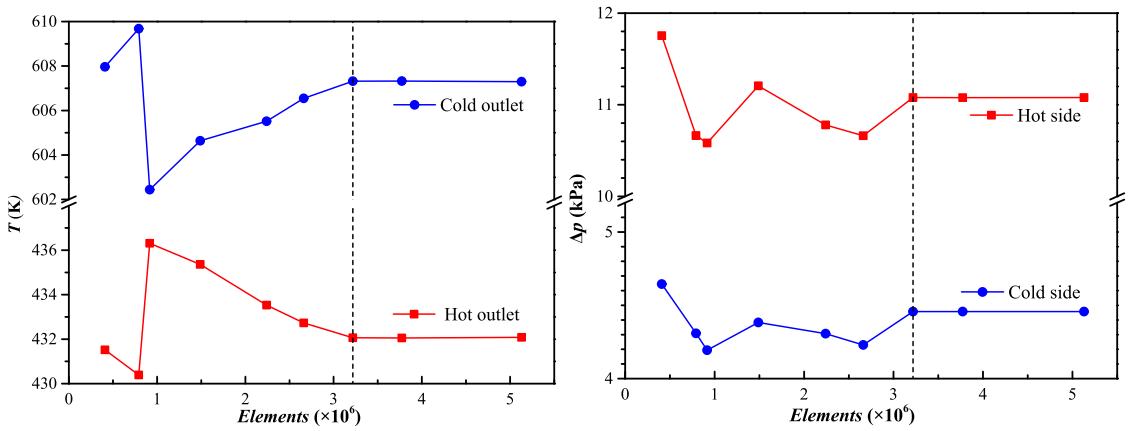

(a) Temperature at the hot outlet and cold outlet. (b) Pressure drop of the hot side and cold side.

Fig. 3. Sensitivity of the grid to the number of elements (Case θ45δ0, Re = 5 000).

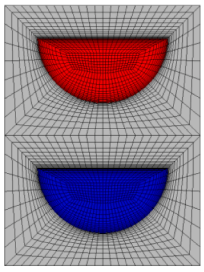

(a) Grid on the cross-section.

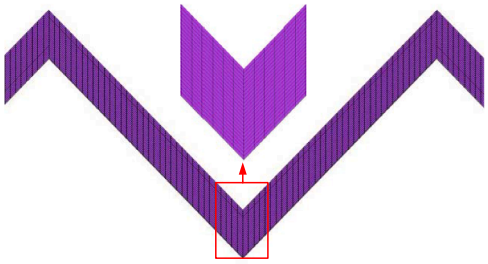

(b) Partial view of the grid for case θ45δ0 in the flow direction.

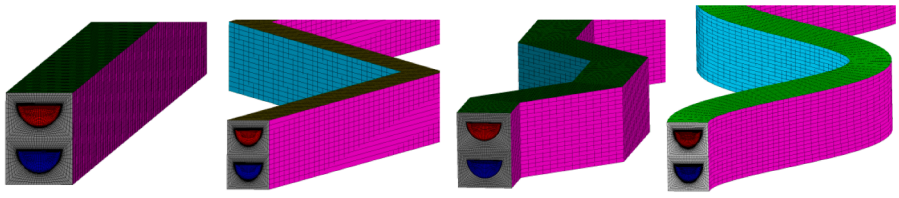

(c) Partial view of the 3D models for case Str, Z45 , M45-0.6 and S45respectively.

Fig. 4. The grid of PCHE unit cell.

30 pitches of 24.6 mm each, the plate thickness of 1.46 mm, the diameter of channel of 1.51 mm. Grid generation and solution methods as aforementioned are employed for simulation. The operating conditions of Kim's experiment are shown in Table 4. In Table 5, a comparison for the numerically and experimentally obtained pressure drop and outlet temperature is given. Both outlet temperature and pressure drop of the present CFD model are observed to match Kim's experimental measurements with reasonable accuracy, the maximum absolute errors are

Table 4
Operating conditions of Kim's experiment.

Case	Operating pressure (bar)	Mass flow rate (kg/s)	$T_{h,in}$ (K)	$T_{c,in}$ (K)
a	18	1.6827×10^{-5}	576.45	335.05
b	18	1.6827×10^{-5}	804.95	354.42

Table 5
Comparison with Kim's experiment.

Case	Parameter	Experiment	Present	$\frac{\lvert Present - Experoment \rvert}{Experiment} \times 100\%$
a	$T_{h,out}$(K)	345.58	347.74	0.63 %
	$T_{c,out}$(K)	563.47	563.80	0.06 %
	Δp_h(kPa)	11.76	11.31	3.83 %
b	$T_{h,out}$(K)	375.34	376.55	0.32 %
	$T_{c,out}$(K)	784.04	782.86	0.15 %
	Δp_h(kPa)	15.32	16.10	5.09 %

0.63 % for temperature and 5.09 % for pressure, respectively.

Thermodynamic properties of S-CO_2 have a higher sensitivity with temperature and pressure than helium. A full-length straight channel PCHE model with S-CO_2 as the working fluid is used to validate the model by comparing it to Meshram's numerical results [44]. The operating temperature, pressure, and the inlet mass flow rate are $T_{c,in} = 400$ K, $P_{c,out} = 22.5$ MPa, $T_{h,in} = 630$ K, $P_{h,out} = 9$ MPa, $m_{c,in} = m_{h,in} = 5.69 \times 10^{-4}$ kg/s, respectively. Both the cold and hot fluids are S-CO_2. As shown in Fig. 5, the temperature variation and the pressure drop of the present study reach quite good agreement with the results reported by Meshram [44]. On the cold flow side, the deviation of temperature between results is less than 0.2 % and pressure drop is less than 4 %, which are considered to be acceptable. Therefore, it can be concluded that the numerical methodology utilized for different channel models with S-CO_2 as the working fluid is reliable and can be used for further study.

3. Results and discussion

3.1. Local performance

3.1.1. Local flow characteristics

To reveal the effects of geometric features on the thermal–hydraulic performance of the modified channel PCHE, the local thermal and flow characteristics of S-CO_2 flow in the straight channels, the zigzag channels and the modified channels are compared and analyzed. The sixth pitch along the hot flow is selected which can avoid the sudden contraction and expansion effects near the inlets and outlets. The sixth pitch is divided into 10 equidistant segments and the 11 cross-sections are used to extract the local information for different cases. The local flow fields including velocity magnitude, flow pathlines, and turbulent kinetic energy on the hot side are shown in Fig. 6.

In Fig. 6(a), the arrow denotes the flow direction in the hot channel. It can be seen that the velocity decreases gradually from the center to the wall in the straight channel. The velocity distribution tends to be non-uniform and unsteady when the configuration moves from the straight channel to the wavy channel and the velocity increases with the increase of the angle in the sixth pitch. For the wavy channels including the zigzag channels and modified channels, the fluid tends to travel the shortest route resulting in some low-velocity areas. For example, before and after the bends in the zigzag channel, there are two areas whose velocity is smaller than the average velocity. In the zigzag channel with an angle of 30° and 45°, a reverse flow after the bends is observed. When the sharp bends are replaced by the straight sections, the pathlines become smoother. The deviation of the average velocity from the center of the channel is reduced. And when the angle is fixed, the modified channel with a larger inserted straight section ratio has much smoother pathlines, resulting in a more uniform flow field. This may cause a reduction in the heat transfer of the modified channel. It can be seen from the legend in Fig. 6(a), the large-angle flow zigzag channel has high-velocity zones after the bends with the same mass flow rate. With the straight section inserted, the high-velocity zones are reduced in the modified channels. In general, the velocity pathlines of the modified channels tend to be more uniform with a smaller pitch angle and larger inserted straight section ratio. The corresponding turbulent kinetic energy distributions in the hot channel are shown in Fig. 6(b). It can be seen that the local high turbulent kinetic energy zones are consistent with the local high-velocity zones. In the straight channel, the turbulent kinetic energy reduces from the center to the wall and it seems that the variation is uniform. It is obvious that the local turbulent kinetic energy increases with the pathlines concentrating in the zigzag channels. These strong turbulence mixing areas are beneficial for the enhancement of the thermal performance whereas they may augment the pressure loss. The modified channels are supposed to destroy the concentration and the thermal–hydraulic performance needs to be further evaluated.

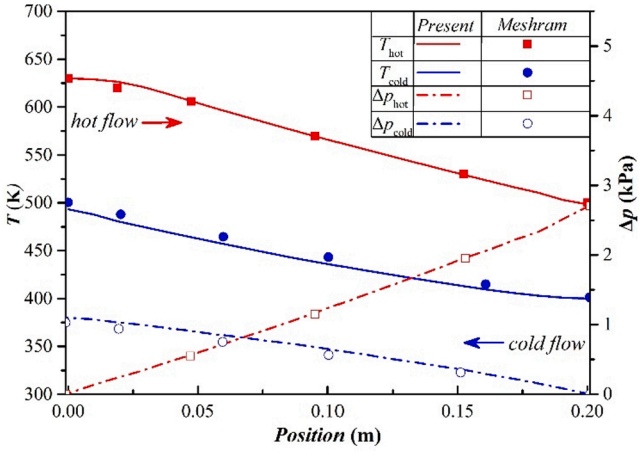

Fig. 5. Comparison with Meshram's results [44].

Fig. 7 shows the pressure loss in the sixth pitch along the flow direction. The pressure loss in the straight channel, from 123 to 147.6 mm along the hot flow direction, remains constant caused by the stable and uniform flow. Due to the flow instability in the wavy channel, large fluctuations in the pressure loss along the flow direction are observed. The fluctuation between the maximum value and the minimum value of the local pressure drop gets larger with the pitch angles increase because of the poor flow stability in the modified channels with large pitch angles. The local pressure drop fluctuation of the zigzag channel is 3.5, 6.7, and 8.6 times the modified channels' when the bend angles are 15°, 30°, and 45°, respectively. The flow in the zigzag channels causes a large pressure drop every time when it encounters a bend. It should be noted that when the angle is 30° and 45° in the zigzag channel, shown in Fig. 7 (c), (d), and (e). There appears a negative local pressure loss in the flow due to the noticeable reverse flow generation revealed in Fig. 6. With the straight section inserted, the fluctuation of local pressure loss is greatly reduced resulted in a much smoother flow. However, the ratio of the inserted straight section only influence the position of the peaks and troughs which are closely related to the location of the bends. The inserted straight section ratio does not have much impact on the range of the local pressure loss.

3.1.2. Local thermal characteristics

Fig. 8. presents the local heat transfer coefficients on both the hot and cold sides in the sixth pitches of all wavy channels. The local heat transfer coefficient is obtained by the following formula:

$$h_\chi = \frac{q_\chi}{T_{w,\chi} - T_{b,\chi}} \tag{9}$$

Where q_χ is the local heat flux of the cross-section inner wall, $T_{w,\chi}$ represents wall temperature (length-weighted average temperature) of cross-section, $T_{b,\chi}$ is the bulk fluid temperature (mass flowweighted average temperature) of the cross-section.

For the straight channel, the local heat transfer coefficients are nearly constant between 123 mm and 147.6 mm. In the wavy channel, oscillations of the local heat transfer coefficients are observed and the amplitude of the oscillations is irregular in most cases. In general, it can

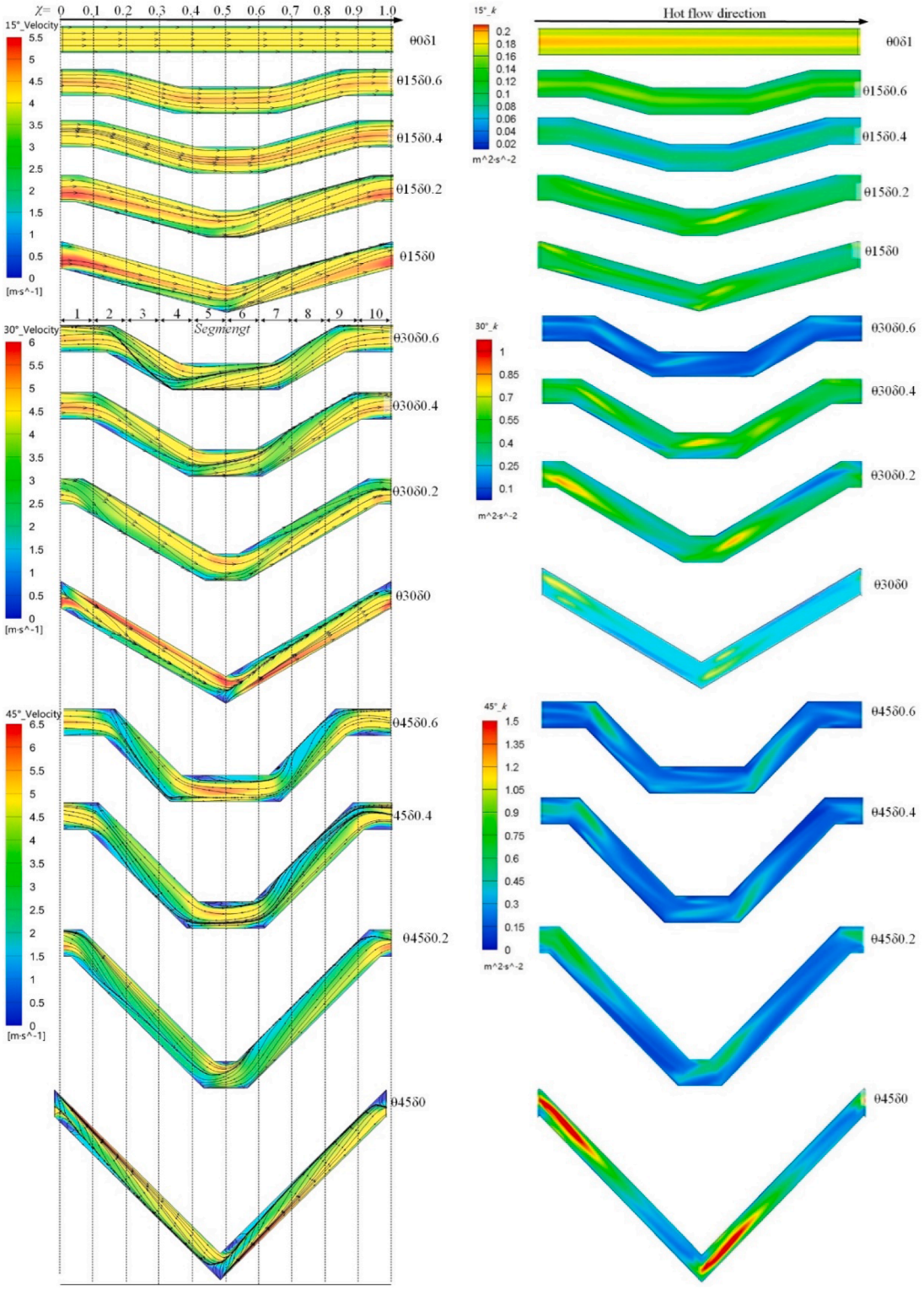

(a) The velocity magnitude and flow pathlines

(b) The turbulent kinetic energy contours

Fig. 6. Flow fields of S-CO_2 in the hot channel. (Re = 15000, 6th pitch for wavy channels, 123 to 147.6 mm for straight channel).

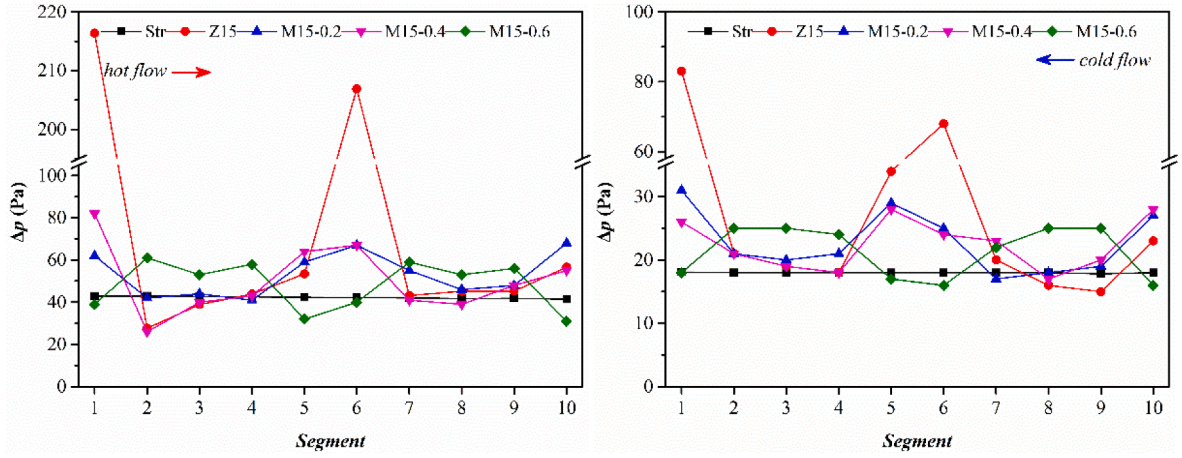

(a) hot flow of bend angle 15° (b) cold flow of bend angle 15°

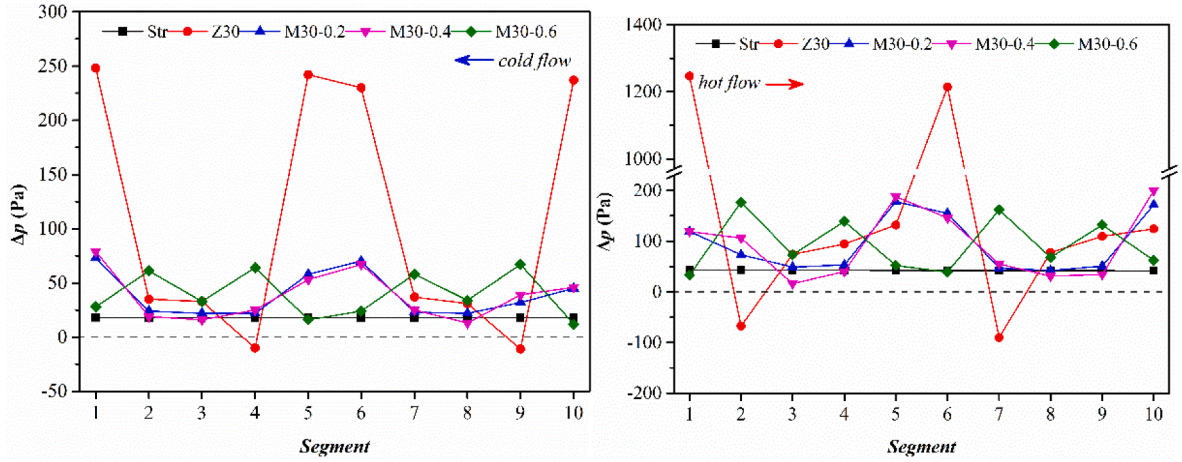

(c) hot flow of bend angle 30° (d) cold flow of bend angle 30°

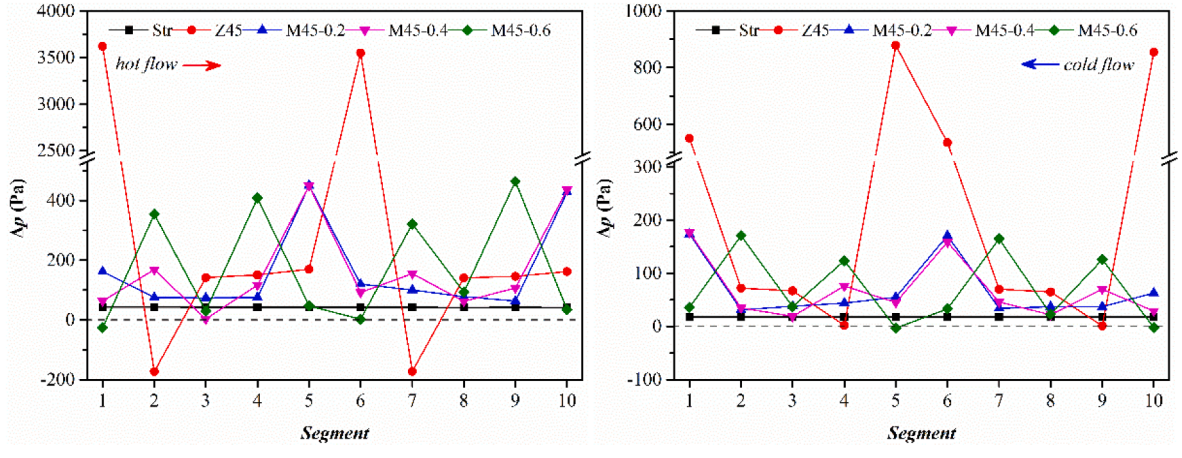

(e) hot flow of bend angle 45° (f) cold flow of bend angle 45°

Fig. 7. The comparison of local pressure loss along the flow direction between the modified channel and the straight channel, zigzag channel. (Re = 15000, 6th pitch for wavy channels, 123 to 147.6 mm for straight channel).

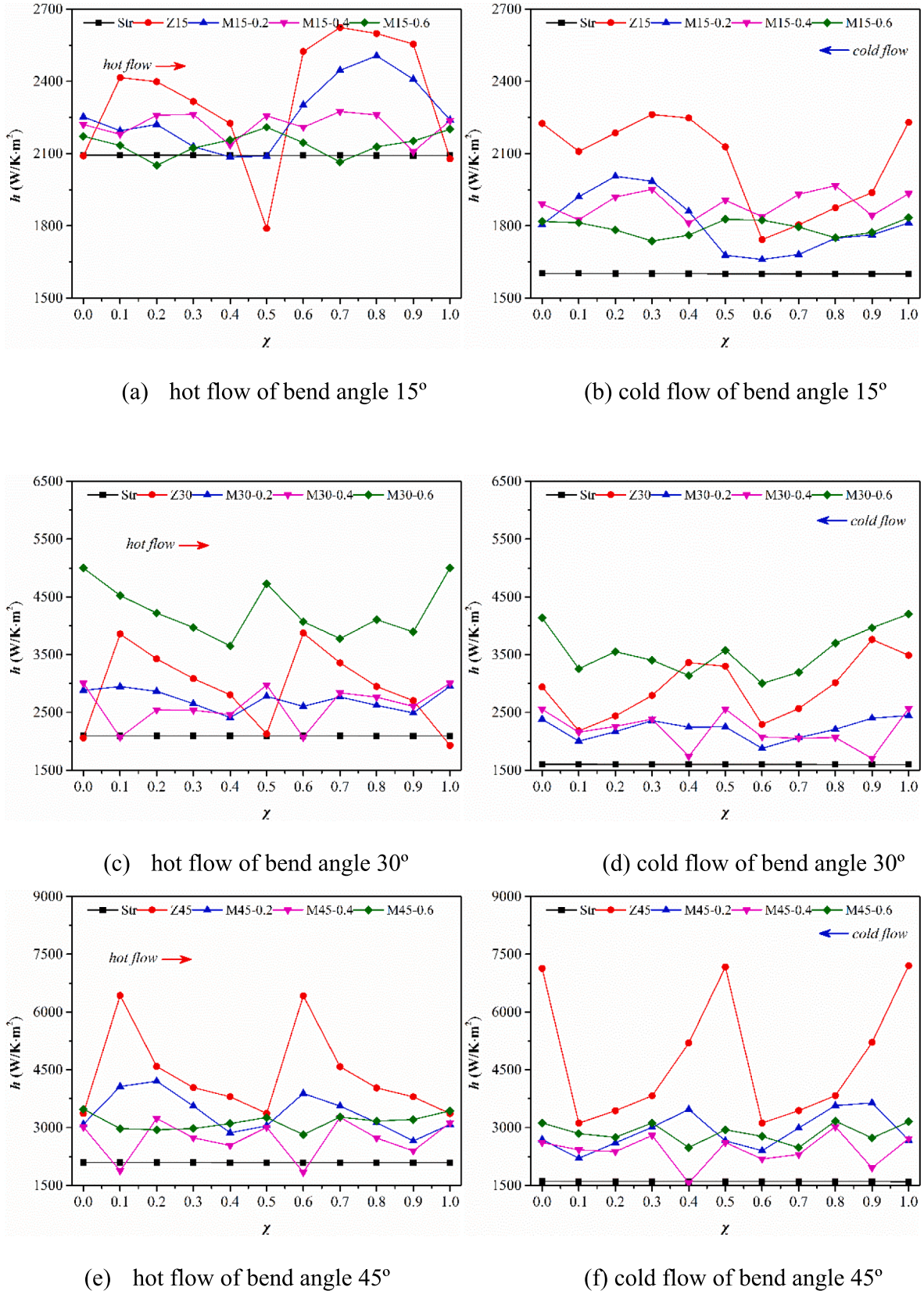

(a) hot flow of bend angle 15°

(b) cold flow of bend angle 15°

(c) hot flow of bend angle 30°

(d) cold flow of bend angle 30°

(e) hot flow of bend angle 45°

(f) cold flow of bend angle 45°

Fig. 8. The comparison of local heat transfer coefficient along the flow direction between the modified channel and the straight channel, zigzag channel. (Re = 15000, 6th pitch for wavy channels, 123 to 147.6 mm for straight channel).

be observed that the majority of local heat transfer coefficients in the wavy channel is higher than those in the straight channel except for very few positions, which suggests as expected that wavy channels are beneficial for heat transfer. For the zigzag channel, the local heat transfer coefficient goes down before the bend then increases considerably around the bend and then decreases in the straight section before approaching to the next bend. This behavior is also observed in the modified channels. With the straight section inserted, the number of bends increases. The local heat transfer coefficients drop first and then rise at every bend. The fluctuations of the local heat transfer coefficients in the modified channels are smaller than those in the zigzag channels, suggesting that S-CO_2 flow in the modified channel is smoother than that in the zigzag channel.

To understand the local thermal performance, the temperature fields of the cross-sections are studied. Fig. 9 shows the temperature contour on the hot sides in the sixth pitches for all cases. In the straight channel, an area with a high temperature in the core is observed at the start and then this phenomenon gradually weakens because the bulk temperature decreases along with the hot flow due to the cooling effect. For the zigzag channel, the fluid temperature distribution tends to be more uniform with the angle increases, which can be explained that the centrifugal force can break the boundary layer and promotes the fluid mixing in the zigzag channel resulting in better heat transfer performance. The larger the pitch angle, the more homogeneous the temperature contour. It can be observed that the temperature gradient gets clearer in the modified channel than that on the zigzag channel. It suggests that the straight section facilitates the smooth passage of the flow which is helpful for pressure loss control but detrimental for thermal performance.

3.2. Overall thermal–hydraulic performance

The global Nusselt number Nu and Fanning friction coefficient f are calculated to evaluate the overall heat transfer and pressure loss characteristics, which can be calculated as Eq.(10) and Eq.(11), respectively.

$$Nu = \frac{h_o D_h}{\lambda} \tag{10}$$

$$f = \frac{\Delta P D_h \rho {A_c}^2}{2m^2 L} \tag{11}$$

where λ, ρ, m represents the thermal conductivity, density, and mass flow rate of S-CO_2 flow, respectively. D_h, A_c, and L is the hydraulic diameter, cross-section area, and length of the centerline of the channel, respectively. The overall pressure loss ΔP and overall heat transfer coefficient h_o are:

$$\Delta P = P_{in} - P_{out} \tag{12}$$

$$h_o = \frac{q_o}{T_{w,o} - T_{b,o}} \tag{13}$$

where q_o is the surface heat flux. The heat flux based on the surface of the fluid domains can be obtained. The minimum heat flux is 27 553.48 W/m^2 in the straight channel when the Reynolds number is 5 000. The maximum heat flux is 133 791.84 W/m^2 in the zigzag channel with a bend angle of 45°when the Reynolds number is 25 000. $T_{b,o}$ and $T_{w,o}$ represent the bulk temperature (or mass flow weighted average temperature) and wall temperature (or area-weighted average temperature) in the fluid domains, respectively.

Fig. 10 indicates the variation of the global Nusselt number and the Fanning friction coefficient for all cases. Generally, the global Nusselt number increases as the Reynolds number increases. The heat transfer performance of the modified channel is higher than the straight channel, while lower than the zigzag channel when the angle is fixed. It can be seen that the gap in heat transfer performance is growing when the angle increases. On the cold side, when the angle is 15°, the modified channels have 5.3 %-11.5 % higher Nusselt numbers than the straight channel and 3.4 %-9.2 % lower Nusselt numbers than the zigzag channel; when the angle is 30°, the modified channels have 15.2 %-34.8 % higher Nusselt

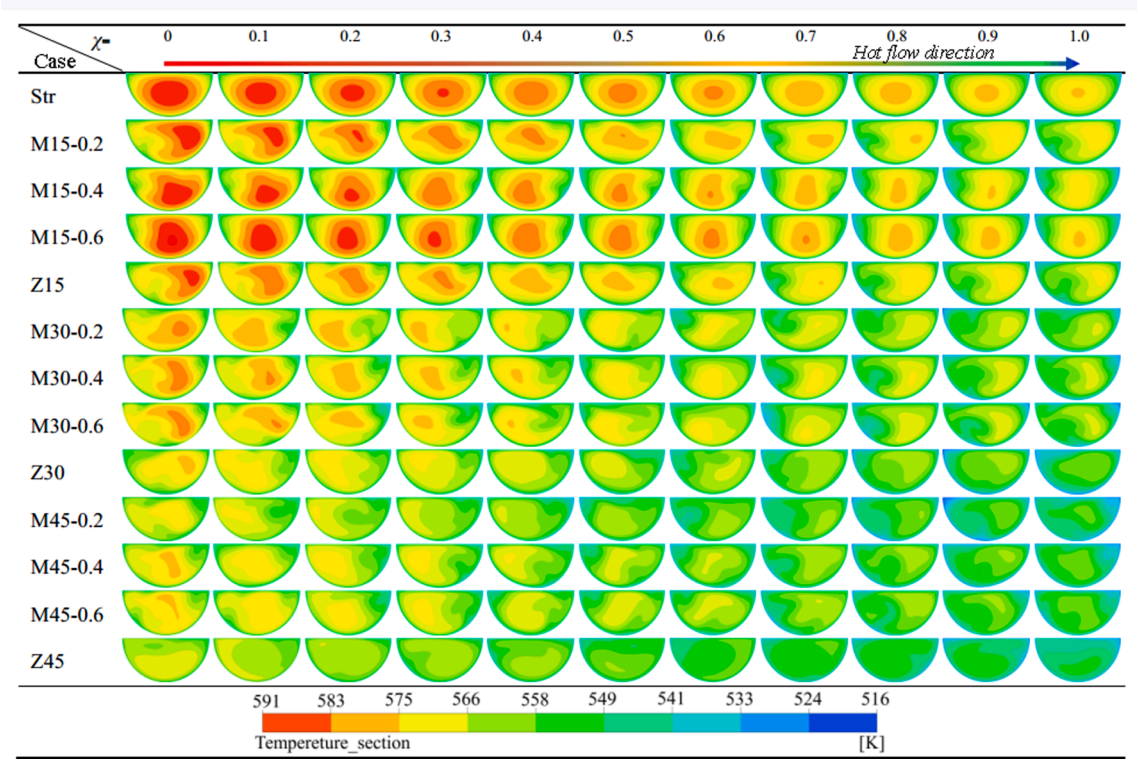

Fig. 9. Temperature distributions of 11 equidistant cross-sections along the hot flow direction. (Re = 15000, 6th pitch for the wavy channels, 123 to 147.6 mm for straight channel).

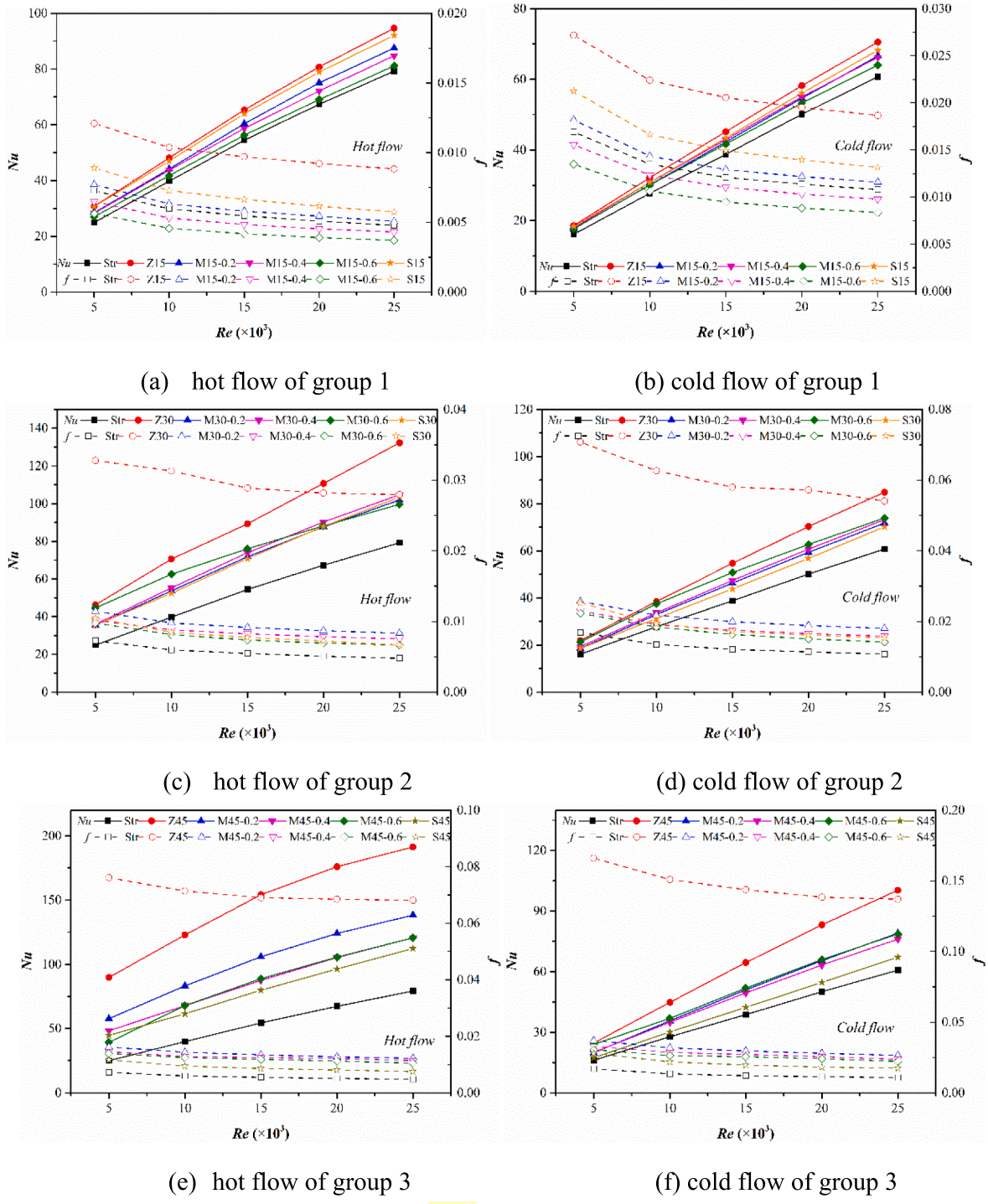

Fig. 10. Comparison of the global Nusselt number and Fanning friction factor between the wavy channels and the straight channel.

numbers than the straight and 2.5 %-15.6 % lower Nusselt numbers than the zigzag channel; when the angle is 45°, the modified channels have 22.8 %-48.7 % higher Nusselt numbers than the straight and 17.7 %-24.2 % lower Nusselt numbers than the zigzag channel. On the hot side, when the angle is 15°, the modified channels have 2.4 %-14 % higher Nusselt numbers than the straight and 7.1 %-14.5 % lower Nusselt numbers than the zigzag channel; when the angle is 30°, the modified channels have 25.7 %-78.7 % higher Nusselt numbers than the straight and 3.5 %-24.7 % lower Nusselt numbers than the zigzag channel; when the angle is 45°, the modified channels have 52.2 %-131.1 % higher Nusselt numbers than the straight and 27.7 %-56.3 % lower Nusselt numbers than the zigzag channel. When compared with the sinusoidal channels,

However, the reverse trend is found in the variation of the global Fanning friction coefficient as the Reynolds number increases. The cold side has a much larger Fanning friction coefficient than the hot side due to the special physical properties of supercritical fluids. The cold flow has much higher density and greater viscosity than the hot flow. The modified channel has a much smoother passage than the zigzag channel, resulting in a very significant drop in the global fanning friction coefficient, which reveals that the inserted straight section is beneficial to pressure loss. By comparison with the zigzag channel, the global fanning

friction coefficient on the cold side of the modified channels decreases 33.1 %-55.2 %, 63.8 %-73.7 %, and 77.8 %-83.8 % when the angle is 15°, 30°, and 45°, respectively. On the hot side, the global fanning friction coefficient on the cold side of the modified channels decreases 36.24 %-58.1 %, 65.1 %-76.2 %, and 78.7 %-84.7 % when the angle is 15°, 30°, and 45°, respectively. Most modified channels have a larger global fanning friction coefficient than the straight channel due to the complexity of the flow passages. However, it is found that when the angle is 15°, the modified channels with an insert ratio of 0.4 and 0.6 have an 8.0 %–23.6 % lower global fanning friction coefficient than the straight channel. This may be caused by the accumulation of lower local pressure loss shown in Fig. 7. (a) and (b). The modified channel has more corners than the zigzag channel, but these corners produce a smoother transition. With these corners, the turbulence disturbance is increased resulting in heat transfer enhancement compared with the straight channel. Meanwhile, these corners prevent the full development of turbulence by destroying the boundary layer, which can reduce the flow resistance.

3.3. Overall assessment

Generally, higher heat performance enhancement is obtained at the cost of pressure loss. PCHE is a heat exchanger that trades-off heat transfer performance with that of pressure loss. Simultaneous assessment of thermal performance and pressure loss aids to find the configuration that has an optimal comprehensive performance. To access the thermal–hydraulic performance of wavy channel PCHE in terms of both heat transfer and pressure loss characteristics compared with the straight channel PCHE, the performance evaluation criteria PEC is employed to evaluate the comprehensive performance [45,46], which is defined as follows:

$$PEC = \frac{Nu/Nu_{str}}{(f/f_{str})^{1/3}} \tag{14}$$

Where Nu_{str} and f_{str} respectively stand for the global Nusselt number and Fanning Friction coefficient of the straight channel PCHE. The PEC of all modified channels and zigzag channels is calculated at different Reynolds numbers, as revealed in Fig. 11.

It can be seen that the PEC of all modified channels is higher than that of zigzag channels with a fixed angle. The PEC on the hot side is always larger than that on the cold side, which is because the Nusselt number on both sides is kept at the same level while the Fanning friction coefficient on the hot side is always lower than that on the cold side. When the Nu/Nu_{str} ratio stays pretty constant, the PEC increases with the decrease of the f/f_{str} ratio. For the cold channel as shown in Fig. 11 (a), the PEC of the zigzag channels are not exceeding 1, and the comprehensive performance of the modified channel is higher than that of the zigzag channel and the sinusoidal channel. Table 6 listed the comprehensive performance enhancement of the modified channels compared to the zigzag channel, which is equal to $\frac{PEC_M - PEC_Z}{PEC_Z} \times 100\%$. Light blue indicates the minimum improvement in cold test performance, and dark blue indicates the maximum improvement in cold test performance. Light yellow represents the minimum value of performance improvement on the hot side, and dark yellow represents the maximum value of performance improvement on the hot side. The modified channels have a 6.9 %-18.3 %, 11.9 %-44.8 %, 24.0 %-29.9 % higher PEC than that of the zigzag channel when the angle is 15°, 30°and 45°, respectively. Among all the channel configurations, case θ30δ0.6 shows the best performance with an improvement of 1.09 and 1.05

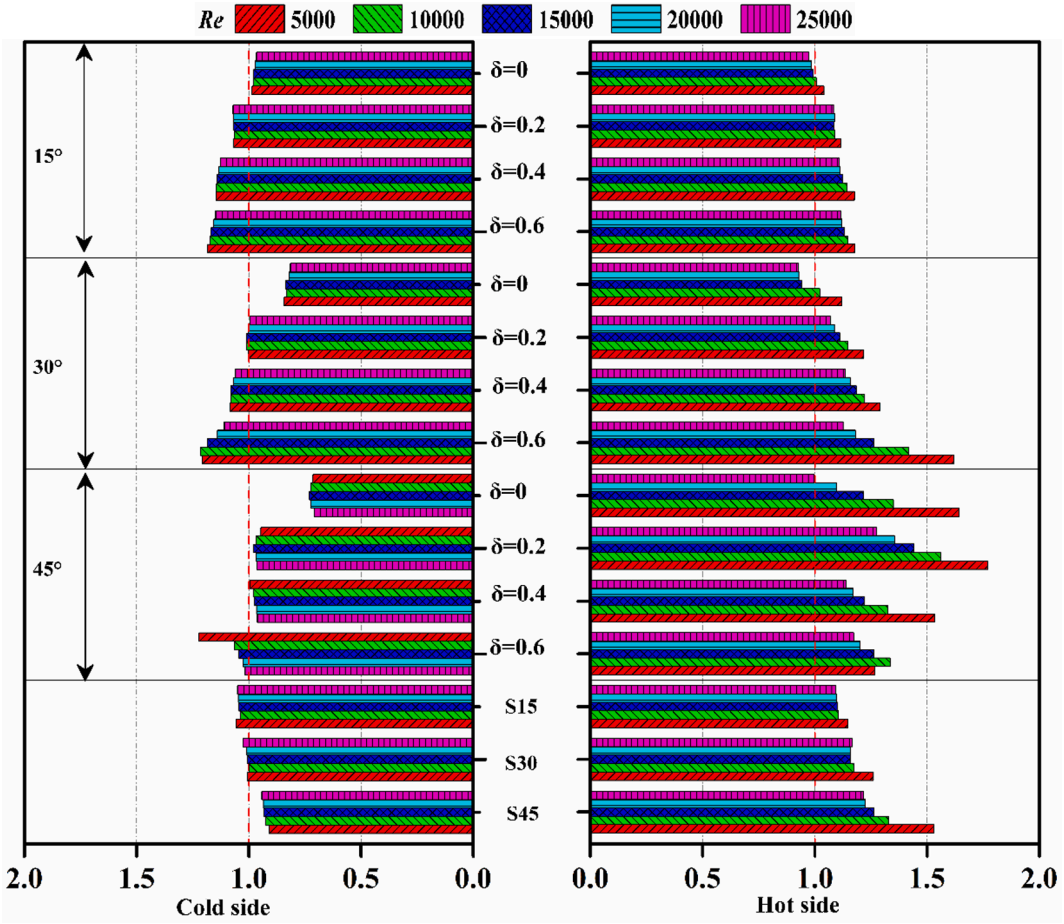

Fig. 11. Comprehensive performance of all cases at different Reynolds numbers.

Table 6
PEC comparison between the modified channel and the zigzag channel.

			$\frac{PEC_M - PEC_Z}{PEC_Z} \times 100\%$				
			Re= 5 000	*Re*= 10 000	*Re*= 15 000	*Re*= 20 000	*Re*= 25 000
15°	0.2	cold	6.9	6.9	7.7	8.6	9.6
		hot	9.3	10.0	11.1	11.9	12.3
	0.4	cold	15.5	15.9	15.9	15.7	15.2
		hot	15.0	15.3	15.2	15.0	15.6
	0.6	cold	18.3	17.9	17.3	16.9	16.2
		hot	17.1	17.3	17.1	16.9	17.4
30°	0.2	cold	11.9	16.8	15.8	17.7	17.3
		hot	18.0	15.4	26.2	22.7	20.3
	0.4	cold	21.7	24.5	23.8	25.5	24.7
		hot	25.1	23.1	34.4	30.7	27.9
	0.6	cold	41.6	44.8	37.3	33.6	29.3
		hot	45.9	38.9	43.5	34.8	29.0
45°	0.2	cold	24.0	26.5	26.9	27.5	30.1
		hot	27.6	28.8	29.2	31.6	33.7
	0.4	cold	24.9	20.8	19.3	19.8	23.1
		hot	24.6	22.4	20.9	23.3	27.3
	0.6	cold	28.5	29.9	26.2	25.5	27.7
		hot	26.6	26.6	27.2	29.3	34.0

when Re = 5 000 and 10,000 respectively, which is 41.7 % and 44.8 % higher than that of the zigzag channel. On the hot side, the comprehensive performance of modified channels is enhanced significantly. It can be seen that almost all the modified channels have a PCE exceeding 1. The modified channels have a 9.3 %-17.4 %, 15.4 %-45.9 %, 20.8 %-34.0 % higher PEC than that of the zigzag channel when the angle is 15°, 30°, and 45° respectively. Same as the cold side, the modified channels have better comprehensive performance than the sinusoidal channel. The advantage of a large insert straight section is more obvious. Among all the channel configurations, case θ30δ0.6 shows the best performance with an improvement of 1.31 compared with case θ30δ0 when Re = 5000, which is 45.9 % higher than that of the zigzag channel. Generally, the hot side has a higher comprehensive performance than the cold side. The PEC increases with the increase of inserted straight section ratio when the angle is 15° and 30°, while there is no obvious enhancement when the angle is 45°. The best comprehensive performance is obtained by a modified channel with an angle of 30°and the insert straight section ratio of 0.6 when Re = 5 000.

4. Conclusions

The present work investigates the thermal–hydraulic characteristics of PCHE with a modified channel based on the zigzag channel by numerical simulation. Various configurations with different angles and inserted straight sections are compared and discussed. The three-dimensional models are validated by both experiments and numerical data from the available literature. Some of the conclusions are as follows:

(1) For the wavy channel PCHE, the introduction of a straight section decreases pressure loss considerably, while at the cost of a limited decrease in thermal performance.
(2) With the straight section inserted, the flow in the modified channel tends to be stable and uniform resulting in the local pressure drop and heat transfer coefficients fluctuating in a smaller range compared to the zigzag channel.
(3) The global Nusselt number and Fanning friction coefficient of the modified channels are within the straight channel and zigzag channel, except for cases M15-0.4 and M15-0.6. The two modified channels with small pitch angles and larger inserted straight section ratios provide better flow characteristics meanwhile increase the thermal performance compared with the straight channel.
(4) In view of the comprehensive performance for wavy channels, the modified channels are consistently higher than the zigzag channels and the sinusoidal channels with the same group. Case M30-0.6, which has the minimum heat transfer performance difference of 2.5 % while greatly reducing the pressure loss of 76.2 %, has the best comprehensive performance, and the PEC is improved by 45.9 % compared to the zigzag channel.

Declaration of Competing Interest

The authors declare that they have no known competing financial interests or personal relationships that could have appeared to influence the work reported in this paper.

Acknowledgments

This work is supported by the High-Tech Ship Research Project of the Ministry of Industry and Information Technology (No. MIIT[2017]614) and the Fundamental Research Funds for the Central Universities(WUT: 2021IUA105). Additionally, Jian Wang would also like to gratefully acknowledge the financial support of the China Scholarship Council (No.201906950017).

Appendix A. Supplementary material

Supplementary data to this article can be found online at https://doi.org/10.1016/j.applthermaleng.2022.119678.

References

[1] V. Dostal, P. Hejzlar, M.J. Driscoll, V. Dostal, P. Hejzlar, M.J.D. High-performance, V. Dostal, P. Hejzlar, M.J. Driscoll, High-Performance Supercritical Carbon Dioxide Cycle for Next-Generation Nuclear Reactors, Nucl. Technol. 154 (2017) 265–282.
[2] E. Sun, J. Xu, M. Li, G. Liu, B. Zhu, Connected-top-bottom-cycle to cascade utilize flue gas heat for supercritical carbon dioxide coal fired power plant, Energy Convers. Manag. 172 (2018) 138–154.
[3] M. Mecheri, Y. Le Moullec, Supercritical CO2 Brayton cycles for coal-fired power plants, Energy. 103 (2016) 758–771.
[4] H. Zhu, K. Wang, Y. He, Thermodynamic analysis and comparison for different direct-heated supercritical CO 2 Brayton cycles integrated into a solar thermal power tower system, Energy. 140 (2017) 144–157.
[5] M.J. Li, H.H. Zhu, J.Q. Guo, K. Wang, W.Q. Tao, The development technology and applications of supercritical CO2power cycle in nuclear energy, solar energy and other energy industries, Appl. Therm. Eng. 126 (2017) 255–275.
[6] O.P. Sharma, S.C. Kaushik, K. Manjunath, Thermodynamic analysis and optimization of a supercritical CO2 regenerative recompression Brayton cycle coupled with a marine gas turbine for shipboard waste heat recovery, Therm. Sci. Eng. Prog. 3 (2017) 62–74.
[7] X. Yan, J. Wang, Y. Sun, C. Yuan, X. Tang, H. Geng, Review on sCO2 Brayton Cycle Power Generation Technology Based on Ship Waste Heat Recovery Utilization, China, Mech. Eng. 30 (2019) 939–946.
[8] J.S. Kwon, S. Son, J.Y. Heo, J.I. Lee, Compact heat exchangers for supercritical CO2 power cycle application, Energy Convers. Manag. 209 (2020), 112666.
[9] B. Zohuri (Ed.), Compact Heat Exchangers, Springer International Publishing, Cham, 2017.
[10] C. Huang, W. Cai, Y. Wang, Y. Liu, Q. Li, B. Li, Review on the characteristics of flow and heat transfer in printed circuit heat exchangers, Appl. Therm. Eng. 153 (2019) 190–205.
[11] W. Chu, X. Li, T. Ma, Y. Chen, Q. Wang, Experimental investigation on SCO2-water heat transfer characteristics in a printed circuit heat exchanger with straight channels, Int. J. Heat Mass Transf. 113 (2017) 184–194.
[12] W. Chu, X. Li, Y. Chen, Q. Wang, T. Ma, Experimental Study on Small Scale Printed Circuit Heat Exchanger with Zigzag Channels, Heat Transf. Eng. (2020) 1–13.
[13] J. Seo, Y. Kim, D. Kim, Y. Choi, K. Lee, Heat Transfer and Pressure Drop Characteristics in Straight Microchannel of Printed Circuit Heat Exchangers, Entropy. 17 (2015) 3438–3457.
[14] F. Pra, P. Tochon, C. Mauget, J. Fokkens, S. Willemsen, Promising designs of compact heat exchangers for modular HTRs using the Brayton cycle, Nucl. Eng. Des. 238 (11) (2008) 3160–3173.
[15] T.L. Ngo, Y. Kato, K. Nikitin, T. Ishizuka, Heat transfer and pressure drop correlations of microchannel heat exchangers with S-shaped and zigzag fins for carbon dioxide cycles, Exp. Therm. Fluid Sci. 32 (2) (2007) 560–570.
[16] M. Chen, J.E. O'Brien, S.J. Yoon, R.N. Christensen, P. Sabharwall, X. Sun, Thermal-hydraulic performance of a high-temperature zigzag-channel printed circuit heat exchanger, Int. Top. Meet. High Temp. React. Technol. HTR 2016 (2016).

[17] M. Chen, X. Sun, R.N. Christensen, I. Skavdahl, V. Utgikar, P. Sabharwall, Dynamic behavior of a high-temperature printed circuit heat exchanger: Numerical modeling and experimental investigation, Appl. Therm. Eng. 135 (2018) 246–256.
[18] M. Chen, X. Sun, R.N. Christensen, Transfer Thermal-hydraulic performance of printed circuit heat exchangers with zigzag flow channels, Int. J. Heat Mass Transf. 130 (2019) 356–367.
[19] Z. Zhao, Y. Zhang, X. Chen, X. Ma, S. Yang, S. Li, Experimental and numerical investigation of thermal-hydraulic performance of supercritical nitrogen in airfoil fin printed circuit heat exchanger, Appl. Therm. Eng. 168 (2020), 114829.
[20] J. Zhou, K. Cheng, H. Zhang, B. Liu, X. Huai, J. Guo, H. Zhang, X. Cui, Test platform and experimental test on 100 kW class Printed Circuit Heat Exchanger for Supercritical CO2 Brayton Cycle, Int. J. Heat Mass Transf. 148 (2020), 118540.
[21] K. Cheng, J. Zhou, H. Zhang, X. Huai, J. Guo, Experimental investigation of thermal-hydraulic characteristics of a printed circuit heat exchanger used as a pre-cooler for the supercritical CO2 Brayton cycle, Appl. Therm. Eng. 171 (2020), 115116.
[22] J.H. Park, J.G. Kwon, T.H. Kim, M.H. Kim, J.E. Cha, H.J. Jo, Experimental study of a straight channel printed circuit heat exchanger on supercritical CO2 near the critical point with water cooling, Int. J. Heat Mass Transf. 150 (2020), 119364.
[23] T. Ma, L. Li, X.Y. Xu, Y.T. Chen, Q.W. Wang, Study on local thermal–hydraulic performance and optimization of zigzag-type printed circuit heat exchanger at high temperature, Energy Convers. Manag. 104 (2015) 55–66.
[24] H. Zhang, J. Guo, X. Huai, K. Cheng, X. Cui, Studies on the thermal-hydraulic performance of zigzag channel with supercritical pressure CO2, J. Supercrit. Fluids. 148 (2019) 104–115.
[25] J. Wang, Y. Sun, M. Lu, J. Wang, X. Yan, Study on the thermal-hydraulic performance of sinusoidal channeled printed circuit heat exchanger, Energy Procedia. 158 (2019) 5679–5684.
[26] S.-M. Lee, K.-Y. Kim, Comparative study on performance of a zigzag printed circuit heat exchanger with various channel shapes and configurations, Heat Mass Transf. 49 (7) (2013) 1021–1028.
[27] S.-M. Lee, K.-Y. Kim, A parametric study of the thermal-hydraulic performance of a zigzag printed circuit heat exchanger, Heat Transf. Eng. 35 (13) (2014) 1192–1200.
[28] P. Taylor, S. Lee, K. Kim, Optimization of zigzag flow channels of a printed circuit heat exchanger for nuclear power plant application, J. Nucl. Sci. Technol. 37–41 (2012).
[29] Z. Wen, Y. Lv, Q. Li, P. Zhou, Numerical study on heat transfer behavior of wavy channel supercritical CO 2 printed circuit heat exchangers with different amplitude and wavelength parameters, Int. J. Heat Mass Transf. 147 (2020), 118922.
[30] A.M. Aneesh, A. Sharma, A. Srivastava, P. Chaudhury, Effects of wavy channel configurations on thermal-hydraulic characteristics of Printed Circuit Heat Exchanger (PCHE), Int. J. Heat Mass Transf. 118 (2018) 304–315.
[31] N. Tsuzuki, Y. Kato, T. Ishiduka, High performance printed circuit heat exchanger, Appl. Therm. Eng. 27 (10) (2007) 1702–1707.
[32] Z. Zhao, K. Zhao, D. Jia, P. Jiang, R. Shen, Numerical investigation on the flow and heat transfer characteristics of supercritical liquefied natural gas in an airfoil fin printed circuit heat exchanger, Energies. 10 (2017).
[33] T.H. Kim, J.G. Kwon, S.H. Yoon, H.S. Park, M.H. Kim, J.E. Cha, Numerical analysis of air-foil shaped fin performance in printed circuit heat exchanger in a supercritical carbon dioxide power cycle, Nucl. Eng. Des. 288 (2015) 110–118.
[34] W. Chu, X. Li, T. Ma, Y. Chen, Q. Wang, Study on hydraulic and thermal performance of printed circuit heat transfer surface with distributed airfoil fins, Appl. Therm. Eng. 114 (2017) 1309–1318.
[35] X. Cui, J. Guo, X. Huai, K. Cheng, H. Zhang, M. Xiang, Numerical study on novel airfoil fins for printed circuit heat exchanger using supercritical CO2, Int. J. Heat Mass Transf. 121 (2018) 354–366.
[36] S. Baik, S.G. Kim, J. Lee, J.I. Lee, Study on CO_2-water printed circuit heat exchanger performance operating under various CO_2 phases for S-CO_2 power cycle application, Appl. Therm. Eng. 113 (2017) 1536–1546.
[37] S.Y. Lee, B.G. Park, J.T. Chung, Numerical studies on thermal hydraulic performance of zigzag-type printed circuit heat exchanger with inserted straight channels, Appl. Therm. Eng. 123 (2017) 1434–1443.
[38] I.H. Kim, H.C. No, Physical model development and optimal design of PCHE for intermediate heat exchangers in HTGRs, Nucl. Eng. Des. 243 (2012) 243–250.
[39] N. Bartel, M. Chen, V.P. Utgikar, X. Sun, I.H. Kim, R. Christensen, P. Sabharwall, Comparative analysis of compact heat exchangers for application as the intermediate heat exchanger for advanced nuclear reactors, Ann. Nucl. Energy. 81 (2015) 143–149.
[40] ANSYS Inc., ANSYS FLUENT 16.0 user's guide, 2015.
[41] E.W. Lemmon, M.L. Huber, M. Mclinden, NIST Standard Reference Database 23: Reference Fluid Thermodynamic and Transport Properties-REFPROP, NIST NSRDS, 2010. Version 9.0,.
[42] I.H. Kim, H.C. No, J.I. Lee, B.G. Jeon, Thermal hydraulic performance analysis of the printed circuit heat exchanger using a helium test facility and CFD simulations, Nucl. Eng. Des. 239 (11) (2009) 2399–2408.
[43] I.H. Kim, Experimental and numerical investigations of thermal-hydraulic characteristics for the design of a Printed Circuit Heat Exchanger(PCHE) in HTGRs, KAIST, 2012.
[44] A. Meshram, A.K. Jaiswal, S.D. Khivsara, J.D. Ortega, C. Ho, R. Bapat, P. Dutta, Modeling and analysis of a printed circuit heat exchanger for supercritical CO2 power cycle applications, Appl. Therm. Eng. 109 (2016) 861–870.
[45] H. Shi, M. Li, W. Wang, Y. Qiu, W. Tao, Heat transfer and friction of molten salt and supercritical CO2 flowing in an airfoil channel of a printed circuit heat exchanger, Int. J. Heat Mass Transf. 150 (2020), 119006.
[46] Z. Zhao, X. Chen, S. Li, S. Yang, L. Huang, Methodology of design and analysis on the thermal hydraulic performance of the cross-flow printed circuit heat exchanger, Int. J. Heat Mass Transf. 156 (2020), 119756.